A refined potential for hydroxylamine clusters and the liquid phase

Alfredo González-Espinoza, Jorge Hernández-Cobos, and Iván Ortega-Blake

Citation: The Journal of Chemical Physics **135**, 054502 (2011);
View online: https://doi.org/10.1063/1.3610344
View Table of Contents: http://aip.scitation.org/toc/jcp/135/5
Published by the American Institute of Physics

A refined potential for hydroxylamine clusters and the liquid phase

Alfredo González-Espinoza,[1] Jorge Hernández-Cobos,[2,a)] and Iván Ortega-Blake[2]
[1]*Facultad de Ciencias, Universidad Autónoma del Estado de Morelos, Av. Universidad 1001, Cuernavaca, Morelos 62290, México*
[2]*Instituto de Ciencias Físicas, Universidad Nacional Autónoma de México, A.P. 48-3, Cuernavaca, Morelos 62251, Mexico*

(Received 25 January 2011; accepted 22 June 2011; published online 1 August 2011)

A detailed study including *ab initio* calculations and classic Monte-Carlo simulations of hydroxylamine in the gas and liquid phases is presented. A classical interaction potential for hydroxylamine, which includes polarizability, many-body effects, and intramolecular relaxation, was constructed. The results of the simulation were compared to the available experimental data in order to validate the model. We conclude that liquid hydroxylamine has a multitude of hydrogen bonds leading to a large density where the existence of *cis* conformers and clusters of these conformers is possible. This explains the occurrence of the classical [R. Nast and I. Z. Foppl, Z. Anorg. Allg. Chem. **263**, 310 (1950)] scheme for the molecule's decomposition at room temperature and its large exothermicity and instability. © *2011 American Institute of Physics*. [doi:10.1063/1.3610344]

I. INTRODUCTION

Hydroxylamine seems to be quite a simple substance, a small molecule comprising the NH_2 and OH chemical groups. It plays an important role in many areas, such as the semiconductor, chemical, and pharmaceutical industries.[2] It is used as a solvent in microchip production to remove organic and inorganic impurities from wafers given its excellent solubility for electrolytes.[3] It is also an important reactive in many organic and inorganic reactions.[4] However, understanding hydroxylamine has been quite a challenge. On the one hand, it is difficult to handle pure hydroxylamine since it is known to decompose at room temperature[5] and even in aqueous solution,[6] which has limited the production of experimental data on this compound. On the other hand, its small size facilitates study by computational and spectroscopic methods.[7–11] It has been found that the hydroxylamine dimer is capable of forming a variety of hydrogen bonds: O–H…O, O–H…N, N–H…N, and N–H…O with single, bifurcated, and even triple character. This has led to a dimer energy surface with several local minima and the expectation that, in the liquid phase, several of these dimers will be playing a role in the decomposition of the substance. In a recent study,[12] the thermal decomposition pathways were examined via *ab initio* calculations of the dimers in the gas phase, using water clusters and a continuum model. However, taking into account the multiplicity of the hydrogen bonds that can be formed between these molecules, it is unlikely that a small number of solvent molecules or a continuum model can yield an accurate description of the molecular image in the condensed phase.

In the past decade, numerical simulations for studying the liquid phase of hydroxylamine were performed.[13–15] In all cases, the studies considered *ab initio* derived potentials. Their results show some discrepancies in the energetics and structure of the liquid phase, but agree in highlighting that the cyclic dimer, which is the optimal dimer in the gas phase, does not seem to be present in the liquid phase. This is a consequence of the hydrogen-bond network in this phase and, therefore, molecular properties such as polarization and intramolecular relaxation can be expected to play an important role. However, none of the previous studies considered the reproduction of these properties and the molecular image can thus be quite different. Numerical simulations that use refined potentials, which include the above degrees of freedom and which are fitted to a good quality *ab initio* surface, are, therefore, necessary and will provide valuable information that is otherwise difficult to obtain for this system.

II. METHODS

Numerical simulations were performed using the Monte Carlo (MC) method. The mobile charge densities in harmonic oscillators (MCDHO) (Ref. 16) potential form was used. This analytical form includes intramolecular relaxation, polarizability, and many-body effects. This potential model has been able to reproduce several water properties quite accurately; the energies, spatial configurations, and dipole moments of clusters, the *ab initio* pair-interaction energies, and the second virial coefficient of liquid phase and steam at various temperatures.[17] It has also been successfully used in the study of other molecular processes; for instance, the hydration of ions,[18–21] the condensed phase of methanol,[22] and the hydration of arsenious acid.[23] Here, a similar type of model for the hydroxylamine interaction with the parameters fitted to reproduce sample points of *ab initio* surfaces was used.

A. The hydroxylamine potential energy and dipole surfaces

The potential energy surface (PES) was constructed at the MP2 level with half counterpoise correction (HCP) using the GAUSSIAN09 program.[24] Half counterpoise correction is

a)Electronic mail: jorge@fis.unam.mx.

TABLE I. *Ab initio* and experimental values of geometrical parameters and dipole moment of the hydroxylamine monomer of minimal energy.

		Ab initio					
	Expt.[a]	6-311++G (*d*,*p*)	aVDZ	6-311++G (2*df*,2*pd*)	6-311++G (3*df*,3*pd*)	aVTZ	CCSD/BSII[b]
r(NO) (Å)	1.453	1.437	1.455	1.444	1.435	1.440	1.449
r(OH) (Å)	0.962	0.960	0.967	0.962	0.959	0.960	0.964
r(NH) (Å)	1.016	1.015	1.024	1.015	1.015	1.010	1.017
<(NOH)°	101.4	101.6	101.6	101.8	102	101.8	102.4
<(HNH)°	107.1	105.9	105.2	105.7	105.7	105.7	106.1
<(HNO)°	103.2	103.6	103.2	103.9	104	103.6	103.5
δ(HNOH)°		124.6	125.4	124.8	124.8	124.8	
θ°	67.3	67.1	68	66.6	66.4	67.1	
μ (D)	0.59 ± 0.05	0.69	0.61	0.63	0.60	0.61	

[a]Reference 31.
[b]BSII = 6-31+G(*d*,*p*). See Ref. 12.

defined as the average value between the corrected and the uncorrected interaction energy values, pretending to compensate the basis set superposition error and diminish the overcorrection produced by full counterpoise. It has been used with good results in systems such as water-water interaction and molecular clusters,[25] and ion-water interactions.[19] Several atomic Gaussian basis sets were tested in order to choose a suitable one that allowed for a large sampling of the potential energy surface at the MP2 level while keeping good accuracy. Table I shows the monomer structure predicted by different basis sets from the literature and experimental data. It is clear that accurate reproduction of the experimental structure requires a large basis set and the CCSD level of theory, but a good approximation can be obtained at the MP2 level and a 6-311++G(2*df*,2*dp*) basis set. It is important to have a proper description of the molecular flexibility, since hydroxylamine is a molecule than can provide multiple hydrogen bonding and, therefore, substantial modifications of the optimal gas phase structure can occur in the condensed phase. The model used here has been used for the description of flexible molecules in the aqueous phase, (e.g., arsenious acid[23]) and we expect it will successfully reproduce this property. A similar analysis on the quality of the basis set size was performed for the optimal dimer interaction of hydroxylamine, and the results are presented in Table II. It can be seen that, after the aug-cc-pVDZ (aVDZ) level, the interaction energy does not change and neither does the optimal structure prediction; hence, it could be a good level for computing a large surface. However, if we look at the dipole moment predictions with different basis sets in Table I it is clear, as expected, that the description of this quantity is difficult. For this reason, we decided to use a basis set which was adequate to treat a large surface and provide a closer approach to the experimental dipole moment; the 6-311++G(3*df*,3*dp*) basis set balances accuracy and computational effort, as can be seen from the comparison of the relative computational cost presented in Table II.

B. Inclusion of the nonadditive effects

As mentioned previously, the MCDHO-type models account for nonadditive effects; we thus fitted the parameters to simultaneously reproduce the hydroxylamine geometrical relaxation, the two-body interaction energy of NH_2OH-NH_2OH, and the three-body nonadditive contributions that appear in $(NH_2OH)_3$ clusters. It has been shown that the energy cost of intramolecular relaxation must be included in the many-body expansion, as proposed by Hankins *et al.*,[26] so that the convergence is achieved when intramolecular relaxation appears.[27] This expansion corresponds to a physical model that considers, first, the deformation of the monomer in vacuum and, then, the interaction of the deformed monomers in the aggregate, i.e.,

$$\Delta E_{(n)} = E_{(n)} - \sum_i E_{(i)} = \sum_i \delta_{(i)} - \sum_{i<j} V_{(ij)} + \sum_{i<j<k} \varepsilon_{(ijk)} + \sum_{i<j<k<l} \varepsilon_{(ijkl)} + \cdots, \quad (1)$$

TABLE II. Geometrical parameters and interaction energies of the minimum energy dimer of hydroxylamine. Distance are in Å, angles are in degrees, and energies are in kcal/mol. CP signifies counterpoise corrected and HCP half counterpoise corrected as defined in the text.

	6-311++G (*d*,*p*)	aVDZ	6-311++G (2*df*,2*pd*)	6-311++G (3*df*,3*pd*)	aVTZ
$r(N–O)_{inter}$	2.843	2.825	2.815	2.810	2.814
$r(H–N)_{inter}$	1.920	1.886	1.884	1.880	1.880
$<(OH–N)_{inter}$	156.7	158.3	158.1	158.0	158.1
$<(NO–N)_{inter}$	85.3	86.4	86.6	86.5	86.4
E_{int}(noCP)	–12.53	–13.36	–12.66	–12.92	–12.85
E_{int}(CP)	–9.83	–10.71	–11.05	–11.24	–11.72
E_{int}(HCP)	–11.18	–12.04	–11.85	–12.08	–12.28
Relative time	1.0	1.6	4.4	8.0	25.8

TABLE III. Three-body nonadditivities for selected trimers with different levels of calculation. Energies are in kcal/mol.

Trimer	1	2	3	4	5
CCSD(T)	–0.70	–2.59	–0.52	0.50	0.49
MP2	–0.71	–2.74	–0.56	0.44	0.37
HF	–0.55	–2.70	–0.57	0.46	0.25

where

$$\delta_{(i)} = E_{(i)}^{(d)} - E_{(i)}, \tag{2}$$

$$V_{(ij)} = E_{ij)} - E_{(i)}^{(d)} - E_{(j)}^{(d)}, \tag{3}$$

$$\varepsilon_{ijk} = E_{ijk} - \sum_{i<j} E_{ij} + \sum_{i} E_i, \tag{4}$$

$$\varepsilon_{ijkl} = E_{ijkl} - \sum_{i>j>k} E_{ijk} + \sum_{i>j} E_{ij} - \sum_{i} E_i, \tag{5}$$

with $E_{(i)}$ being the energy of the molecule in its minimum energy structure, $E_{(i)}^{(d)}$ being the energy of the distorted monomer, and $E_{i,n}$ being the total energy of a cluster of n molecules. Since NH_2OH is a neutral molecule, nonadditivities are certainly smaller than those of divalent single ions[28,29] and those of monovalent ions[18,19] computed using the same scheme, but they have to be included for an accurate description of the overall interaction energy. Four-body nonadditive corrections were also calculated and we found that these and higher-order terms can be safely neglected since, for instance, the four-body contributions of the minimum energy tetramer are less than 0.05% of the total interaction energy.

To address the point of how these contributions vary with the level of calculation we present the nonadditive energies for a small set of trimers at the CCSD(T), MP2, and SCF levels. The results presented in Table III show that the predictions at the different levels are similar, in agreement with the expectation that, for polar systems, nonadditivity is dominated by the effects sufficiently well modeled at the SCF level of theory.[30] Nonetheless, the maximal difference between SCF and CCSD(T) is about 50% of the latter value, whereas the corresponding maximal difference at the MP2 level is about 25%. Thus, we considered the nonadditivities at the MP2 level, but of course we have to bear in mind that these differences are normally within the fitting error.

Thus, in order to fit the parameters for the hydroxylamine potential, the PES was built in two stages. In the first stage, a large number of points in the intramolecular monomer surface were calculated varying the different internal degrees of freedom. The corresponding energies for the different geometries were referred to the energy of the minimum-energy structure of hydroxylamine. The two-body surface was calculated starting with several dimers and varying the distance between their molecules, rotating the orientation of one molecule in relation to the other, and rotating one molecule around the other, thus exploring both the repulsive and the attractive regions. Special care was taken to explore the different hydrogen-bond interactions. We did several energy minimizations starting from arbitrary initial configurations that converge into the hydrogen-bond configurations. In the same way a number of points in the hydroxylamine three-body nonadditive surface were also calculated, that is, by optimizing several trimers sampling the different HB-arrangements that would lead to different three body local minima. With the surfaces thus constructed, the parameters of the potential were fitted. In the second stage and using the parameters from the first stage, we performed MC simulations allowing for variations of all degrees of freedom in order to produce random structures of hydroxylamine aggregates, the interaction energies, and nonadditivities of these aggregates were then calculated at the MP2/6-311++G(3*df*,3*pd*) level and added to the previous PES. The potential was then refitted until the new aggregates were reproduced with the same accuracy as those of the previous PES. A similar procedure was performed in order to obtain random structures from MC simulations of the liquid state. The resulting potential energy surfaces computed at the MP2/6-311++G(3*df*,3*pd*) level include 3816 monomers, 3813 dipole values for these geometries, 3350 pair interactions, and 333 three-body nonadditivities. All the geometries, *ab initio* energies, and dipole moments were included in the supplementary material accompanying this work.[43]

C. Analytical potentials

It is important that all the care taken in building the intramolecular and the intermolecular interactions is not lost when going to the classical potential used in the MC simulations. The MCDHO scheme, in which two kinds of interactions (intramolecular and intermolecular) are defined, was used for the construction of the analytical potential. In the MCDHO model, presented in detail in Refs. 16 and 22, a molecule is generally represented by a negative mobile charge density with radial exponential decay attached to a positively charged point core by a harmonic oscillator for each of its atoms. The specific expressions for the interactions in the MCDHO model are given in Eqs. 6–16 of Ref. 16. In this work, which is similar to the study of arsenious acid,[23] we have introduced some changes: the terms $A_{ij}r^{-6} + B_{ij}r^{-12}$ in the intermolecular interaction were substituted by $A_{ij}\exp(\alpha_{ij}r) + B_{ij}\exp(\beta_{ij}r)$ since they yielded better agreement with the potential energy surface. Furthermore, in order to get a better reproduction of the two-body energy it was necessary to give greater flexibility to the potential, mainly, so that the hydrogen bond interactions N–H…O and N…H–O could be reproduced equally well. We found that having two charges attached to the oxygen atom by independent springs, and lacking any interaction between them, resulted in a better reproduction of this surface. The functional form of the model potential was included in the supplementary material of this work.[43]

The reproduction by the classical model of the *ab initio* energy surface corresponding to different configu-

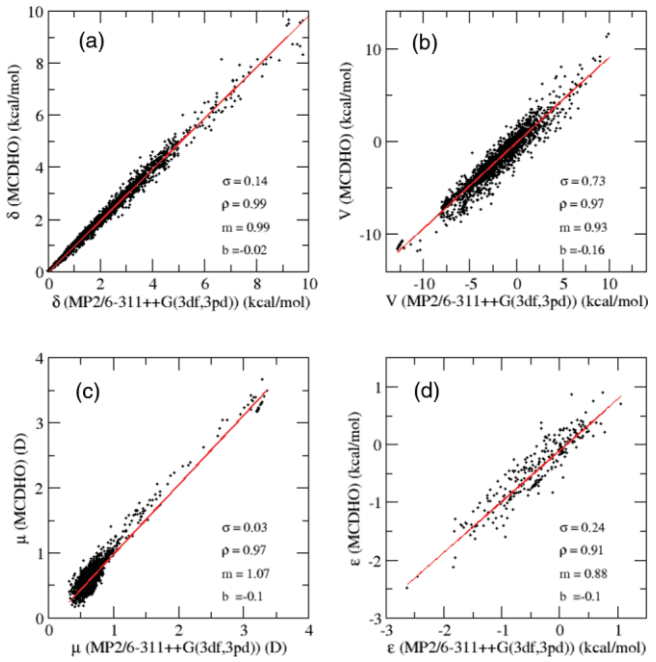

FIG. 1. Reproduction of the energy and dipole surfaces computed at the *ab initio* level using the model with the parameters presented in Table III. The values corresponding to δ, V, and ε correspond to Eqs. (2)–(4) from the text.

rations of NH_2OH is presented in Fig. 1(a), which shows that this reproduction is rather good, both in the correlation as well as presenting a small dispersion of the values in spite that structural variations of both (*trans* and *cis* monomers) are considered. Figure 1(b) shows the reproduction of the dipole moment of hydroxylamine monomers. Again, it is a successful reproduction with a small dispersion and an adequate description of the dipole moment of the *trans* and *cis* monomers. Figure 1(c) shows the reproduction of the hydroxylamine dimer interaction as described in Eq. (3); the correlation is good but there is some dispersion in spite of having given extra flexibility to the analytical form by considering two density charges on the oxygen atom. To quantify this dispersion, we calculate the deviation of the energies predicted by the model potential in the low-energy range and found that there is an average of 10% deviation in this region. We think that the ability of nitrogen and oxygen to act as donor and acceptors in hydrogen bonds between oxygen-oxygen, oxygen-nitrogen, and nitrogen-nitrogen is a condition that seems to require further complexity of the model and the inclusion of additional physical phenomena rather than extra mathematical flexibility. However, it should be noted that there is agreement in the interaction energies of the minimum-energy dimers presented in Table VI, but a discrepancy in the optimal geometries. This indicates that the model potential is predicting geometries that are slightly different from the *ab initio* ones.

Figure 1(d) shows the reproduction of the three-body nonadditivity. It can be seen that this contribution is small and reasonably well reproduced by the model. Table I of the supplementary material of this work shows the set of parameters that produced the mentioned reproductions.[43]

III. RESULTS

A. Properties of monomers and small clusters

In order to check the performance of the model we compared the experimental, *ab initio*, and model predicted molecular properties of the minimum-energy aggregates. Table IV shows the geometrical parameters for the minimum energy configurations of the *cis* and *trans* monomers. It can be seen that there is a good agreement with the experimental values of Tsunekawa[31] and, of course, a better agreement with the *ab initio* values. A similar result is observed for the dipole moment of the molecules and the energy difference between both structures, favoring the *trans* form by 4.2 kcal/mol, which also agrees with *ab initio* calculations performed with a higher level of computation.[12] Table V shows a comparison of the experimental gas phase,[32] Ar matrix,[33] *ab initio* and model potential vibrational frequencies of hydroxylamine. The model vibrational frequencies were calculated using the normal mode analysis in the minimum energy monomer predicted by the model potential. The force constants were determined numerically using centered differences to calculate the second derivatives. As can be seen, there is a good agreement with the *ab initio* values and the discrepancies with the experimental values are those appearing at the *ab initio* MP2 level.

TABLE IV. Values of the geometrical parameters and dipole moments for the *trans* and *cis* hydroxylamine minimum energy monomers. The relative energy difference between these monomers is also shown.

	trans			*cis*	
	Expt.[a]	6-311++G(3*df*,3*pd*)	MCDHO	6-311++G(3*df*,3*pd*)	MCDHO
r(NO) (Å)	1.453	1.435	1.437	1.437	1.434
r(OH) (Å)	0.962	0.959	0.959	0.960	0.959
r(NH) (Å)	1.016	1.015	1.015	1.013	1.012
<(NOH)°	101.4	102.0	102.3	107.7	107.0
<(HNH)°	107.1	105.7	106.1	107.7	108.4
<(HNO)°	103.2	104.0	104.2	106.7	106.6
δ(HNOH)°		124.8	124.6	57.4	57.8
θ°	67.3	66.4	66.0	119.0	119.2
μ (D)	0.59 ± 0.05	0.60	0.54	3.08	3.21
ΔU (*trans*- *cis*) (kcal/mol)	*Ab initio* = 4.21	MCDHO = 4.23			

[a]Reference 31.

TABLE V. Vibrational frequencies predicted by the *ab inito* calculations (MP2/6-311++G(3*df*,3*pd*)) and the model potential compared to their experimental counterparts. Values are in cm^{-1}.

	Expt. gas phase[a]	Expt. Ar matrix[b]	*Ab initio*	MCDHO
ν(O–H) A′ ν_1	3649.89	3634.7	3886.0	3785.9
ν(N–H) A″ ν_7	3358.76	3353.3	3601.0	3642.5
ν(N–H) A′ ν_2	3294.25	3289.7	3510.3	3609.8
$\delta(NH_2)$ A′ ν_3	1604.52	1598.9	1666.7	1682.0
δ(NOH) A′ ν_4	1353.3	1350.7	1396.6	1349.5
$\rho_t(NH_2)$ A″ ν_8	1294.5		1342.6	1330.2
$\rho_w(NH_2)$ A′ ν_5	1115.47	1117	1155.0	1168.2
ν(N–O) A′ ν_6	895.21	895.9	955.9	983.1
Torsion A″ ν_9	385.96	375.9	420.5	455.7

[a]Reference 32.
[b]Reference 33.

Figure 2 shows the structure of the minimum energy dimers constructed with *trans-trans*, *cis-cis*, and *trans-cis* monomers. There is a good overlap between the model and the *ab initio* predicted structures. The root mean square deviation (rmsd) values are presented in Table VI together with some characteristic distances that are useful for understanding the radial distribution functions. The interaction energies of the aggregates at the a*b initio* and model level were also compared and found to be in a good agreement.

B. Condensed phase

We carried out MC simulations using the Metropolis algorithm,[34,35] considering 500 hydroxylamine molecules in a cubic computational cell. The initial configuration of the hydroxylamine system was generated using the PACKMOL package.[36] Simulations over a NPT ensemble were performed to determine the density predicted by the model. The system was equilibrated for 250×10^6 configurations and the next 250×10^6 configurations were taken as the statistical sample for further analysis. Such long simulations are required to ensure that equilibrium has been attained and the sample is statistically meaningful, i.e., simulation times are considerably longer than the correlation period. Monte Carlo methods or molecular dynamics typically produce raw data in the form of finite time series of correlated data. Hence, simulation times simply means the length of the Monte Carlo run, large enough to decorrelate the sampling configurations with the initial one. The quantitative assessment of these conditions was made with the blocking method of Flyvbjerg and Petersen.[37] A spherical cutoff of 14.13 Å and toroidal periodic boundary conditions were used. The long-range Coulomb interaction was corrected via Ewald sums.[38] The predicted density as a function of temperature is shown in Table VII and compared to the experimental counterpart, showing a good prediction with a 4% error. The vaporization enthalpy can also be compared and was computed as $H_{vap} = U_{vap} - U_{liq} + RT$. U_{vap} is the energy of the vapor phase which was calculated with a Monte Carlo simulation at the corresponding temperatures using 25×10^6 configurations for equilibration and 25×10^6 configurations to obtain the average energy of the system. U_{liq} was computed as the average of the interaction energy per molecule of the liquid hydroxylamine system predicted by the MCDHO potential in a simulation of 500 molecules. The experimental value of the vaporization enthalpy was determined by Back and Betts[39] from the vapor pressure data. Although a good estimation of the vaporization energies is a rather difficult task for both theoretical and experimental determinations, the value obtained in this work, 11.12 kcal/mol, is very close to the experimental estimation of 11.4 kcal/mol. This good agreement between our theoretical value and the experimental one, which could be fortuitous, rewards the effort put into the reproduction of the MP2/6-311++G(3*df*,3*pd*) potential energy and dipole surfaces by the classical model. The experimental dipole moment of the molecule compares well to the corresponding theoretical gas phase value, but the average liquid phase dipole moment of the molecule is completely different. If we look at the average geometrical structure that occurs in the liquid phase at different temperatures compared to the gas phase (Table VII), we will see substantial differences in the angles formed with the hydrogen atoms. This indicates an effect of the hydrogen bond network and is more marked in the dihedral angle. If we compare these average structures with those corresponding to the minimum-energy *cis* and *trans* monomers presented in Table V, it is clear that the *trans* monomer is present in the gas phase whereas the *cis* monomer is also present in the liquid phase. The average dipole moment observed in the liquid is also close to the one corresponding to the *cis* monomer.

In order to verify that there is a preferred occurrence of the *cis* monomer in the liquid phase; Fig. 3 shows a histogram of the probability of appearance of the different values of the dihedral angle in a simulation of a liquid hydroxylamine at 45 °C. This histogram was constructed using a 50×10^6 configurations of the simulation. Two broad distributions

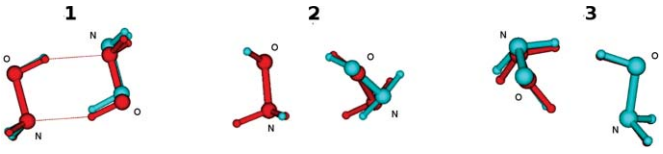

FIG. 2. Minimum-energy dimers constructed with the *trans* and *cis* monomers. The *trans-trans* dimer (1), the *cis-cis* dimer (2), and the *trans-cis* dimer (3). The geometries in red correspond to the *ab initio* minimal energy predicted structures and the ones in blue those of the model.

TABLE VI. Comparison between *ab inito* (6-311++G(3*df*,3*pd*)) and model potential minimum energy clusters. Dimers where constructed with the *cis* and *trans* monomers. Trimer and tetramer are constructed with *trans* monomers.

	Dimer						Trimer		Tetramer	
	trans-trans		*cis-cis*		*trans-cis*		*trans-trans*		*trans-trans*	
	Ab initio	Model	*Ab initio*	Model	*Ab initio*	Model	*Ab initio*	Model	*Ab initio*	Model
rmsd (Å)	0.08		0.17		0.07		0.03		0.08	
r(O–O)	3.233	3.165	2.875	2.861	2.802	2.869	3.849	3.850	3.32	3.301
r(O–N)	2.812	2.853	3.412	3.633	3.352	3.371	2.796	2.763	3.027	3.050
	2.812	2.850	2.906	2.950	2.772	2.874				
r(N–N)	3.075	3.224	3.092	3.370	3.390	3.481	3.571	3.514	3.390	3.434
r(O–H_O)	2.573	2.492	2.081	2.007	2.006	2.081				
		2.494	3.275	3.135	2.453	2.533				
r(O–H_N)	3.460	3.540	2.458	2.488	2.849	2.848				
		3.531	2.905	3.281	3.461	3.576				
		3.532	3.790	3.904	3.479	3.586				
		3.533	3.881	3.969	4.055	4.102				
r(N–H_O)	1.884	1.916	2.510	2.413	1.985	2.107				
		1.920	4.089	4.173	2.674	2.688				
r(N–H_N)	3.780	3.920	2.370	2.754	2.959	3.016				
		3.921	2.871	3.047	3.753	3.860				
		3.925	3.751	3.971	3.761	3.893				
		3.925	4.070	4.354	4.296	4.395				
r(H_O–H_O)	2.169	2.069	2.522	2.403	1.940	2.019				
r(H_N–H_O)	2.533	2.616	2.335	2.259	2.402	2.394				
r(H_N–H_N)	4.298	4.455	2.402	2.620	3.106	3.183				
E_{int}(kcal/mol)	–12.1	–12.0	0.5	0.5	– 4.4	– 4.4	– 20.8	– 20.1	– 28.1	– 26.6

around the values corresponding to the dihedral angle of the *cis* and *trans* monomers appear. The broadness of the distributions emphasizes how the hydrogen bond network affects these angles but, most importantly, the histogram shows that the *cis* monomer is dominant. Adjusting Gaussian functions to the profile and obtaining the corresponding areas for the Gaussian in the *cis* and the *trans* region estimates a relative probability of 59.34% for the *cis* monomer and 40.65% for the *trans* monomer. A further analysis on the relative probability is performed in the simulation of a cluster of 100 hydroxylamines at 45 °C. Figure 3 shows the relative probability as a function of the location of the molecule in the cluster. The position of the molecule is defined relative to the center of mass of the cluster and the histogram was constructed during a 100×10^6 configuration simulation. There is a dominance of the *trans* monomer at the surface of the cluster, which diminishes steadily as one moves to the center. It is clear that the solvent effect is the one responsible

TABLE VII. Predicted properties of liquid hydroxylamine at different temperatures and comparison to the experimental values.

	Expt.		MC simulation					
	Gas	Liquid	Gas	Liquid	Gas	Liquid	Gas	Liquid
Temperature (°C)	25	33	32.05	32.05	45	45	110	110
r(NO) (Å)	1.453[a]		1.442	1.447	1.443	1.447	1.444	1.447
r(OH) (Å)	0.962[a]		0.961	0.972	0.962	0.973	0.962	0.972
r(NH) (Å)	1.016[a]		1.018	1.026	1.018	1.025	1.019	1.026
<(NOH)°	101.4[a]		102.3	105.0	102.2	105.0	102.1	104.3
<(HNH)°	107.1[a]		105.7	102.7	105.7	102.7	105.6	102.4
<(HNO)°	103.2[a]		104.8	104.3	104.0		103.9	104.0
δ(HNOH)°			124.6	77.6	124.6	75.2	124.6	94.7
μ (D)	0.59 ± 0.05[a]		0.7	3.6	0.8	3.7	0.8	2.7
ΔU (kcal/mol)			2.70	–7.82	2.90	–7.56	3.50	–6.1
ΔH_{vap} (kcal/mol)	11.4[b]	11.12	11.09	10.30				
ρ(g/cm^3)		1.204[c]		1.247		1.237		1.132

[a]Reference 31.
[b]Reference 29.
[c]Reference 3.

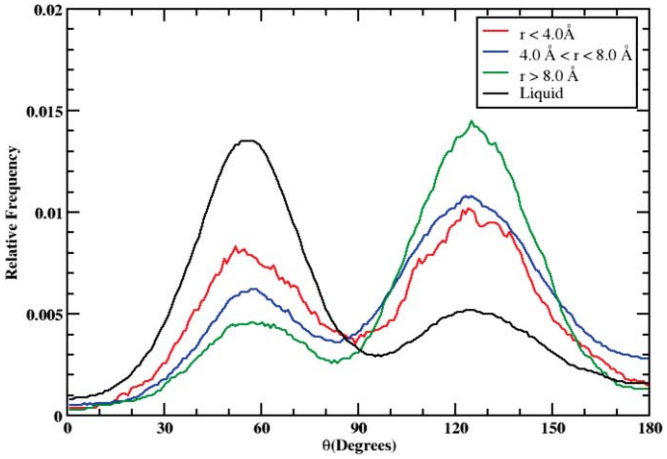

FIG. 3. Dihedral angle distribution. The black line corresponds to the liquid hydroxylamine at 45 °C, the rest to monomers in a cluster of 100 molecules at 45 °C. Red stands for monomers in a sphere of 4.0 Å radius, blue for monomers in shell between 4.0 and 8.0 Å, and green for molecules at distances larger than 8.0 Å.

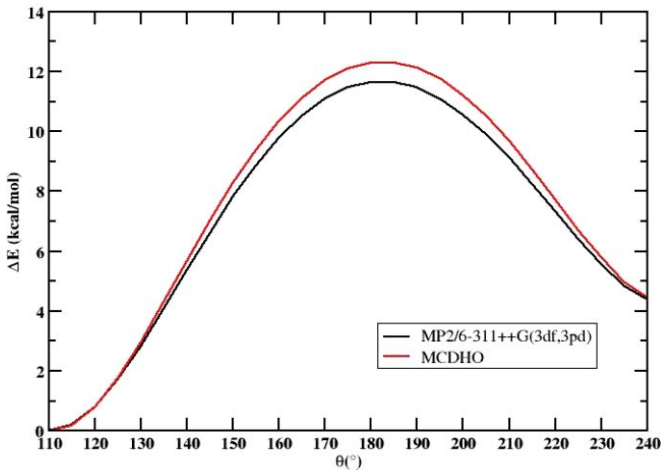

FIG. 4. *Ab initio* and model potential energy barrier for the inversion of the amino group. θ is the angle between the O–N vector and the dipole vector of the amino group.

for the change from one monomer conformation to the other.

To further investigate the causes of this behavior, we performed Polarizable Continuum Model (PCM) (Ref. 40) calculations with hydroxylamine as a solvent for both conformers, *trans* and *cis*. Solvation energy stabilizes both conformers, more the *cis* than the *trans,* but still the latter is the most stable one by 1.66 kcal/mol.

To determine the solvation energy of the *trans* and *cis* conformers coming from Monte Carlo simulation we assumed that the dihedral angle distribution of conformers presented in Fig. 3 represents the probability of finding a particular conformer of hydroxylamine solvated by hydroxylamine. Assuming that this is a Boltzmann distribution and knowing the average solvation energy of hydroxylamine ($\langle E_{solv}\rangle$) we can determine the solvation energy of any conformer ($\langle E^i_{solv}\rangle$) in the distribution. The difference between the solvation energies of two conformers is given by

$$\Delta E^{ij}_{solv} = -kT \log\left(\frac{\rho_i}{\rho_j}\right) \tag{6}$$

where ρ_i and ρ_j are the relative probability values of this conformers in the distribution of Fig. 3. Also the average solvation energy of hydroxylamine is equal to

$$\langle E_{solv}\rangle = \sum\nolimits_i \rho_i E^i_{solv}. \tag{7}$$

We then propose a value for solvation energy of a reference conformer; thus, permitting the computation of $\langle \Delta E^{ij}_{solv}\rangle$ (using Eq. (6)) and $\langle E_{solv}\rangle$ (using Eq. (7)). If the condition that $\langle E_{solv}\rangle$ is equal to the value of the average solvation energy obtained in the Monte Carlo simulation is imposed, we can obtain the solvation energies of the *trans* and *cis* conformers as those corresponding to the maxima of each peak in the distribution of Fig. 3.

The results obtained were –11.0 kcal/mol and –11.6 kcal/mol for the *trans* and *cis* conformers, respectively. The solvation energies of both conformers calculated using the PCM method, –6.6 kcal/mol for *cis* and –4.0 kcal/mol for the *trans* conformer, are quite different. This is clearly a consequence of the lack of the hydrogen bonding contributions in the PCM model. This was confirmed by an analysis of the interaction energies of conformers close (±5°) to the *trans* and *cis* configurations in the Monte Carlo simulation. We found that the interaction energies with the nearest neighbors (any intermolecular distance less than 2.2 Å) are considerably more favorable for the *cis* conformer, even to the point of compensating the associated deformation energy. Also, as expected, the interaction with the far away molecules is more favorable to the *cis* conformer due to its larger dipole moment. Thus, the geometry change produced by the solvent is due to both contributions but more markedly to the hydrogen bonding.

It has been argued (Visozo *et al.*[41]) as a known fact that only the *trans* conformer is present in liquid hydroxylamine. However, no experimental evidence is given in that work and, to the best of our knowledge, there is no such experimental evidence. Visozo *et al.*[41] also argued that for the Na^+–NH_2OH complex the rearrangement of H-bonds associated with this

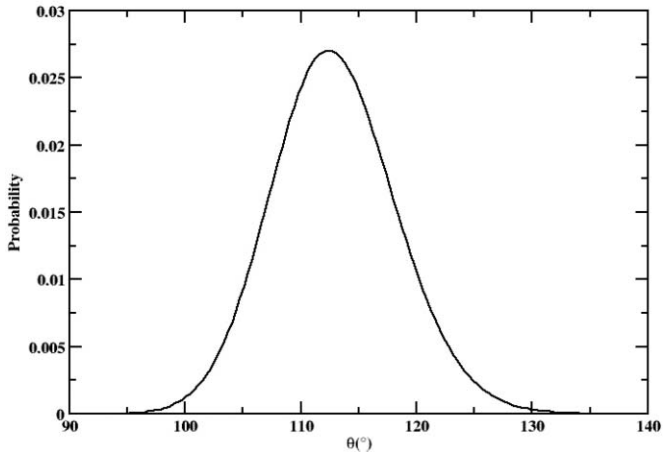

FIG. 5. Probability of the occurrence of the angle between the O–N vector and the dipole vector of the amino group.

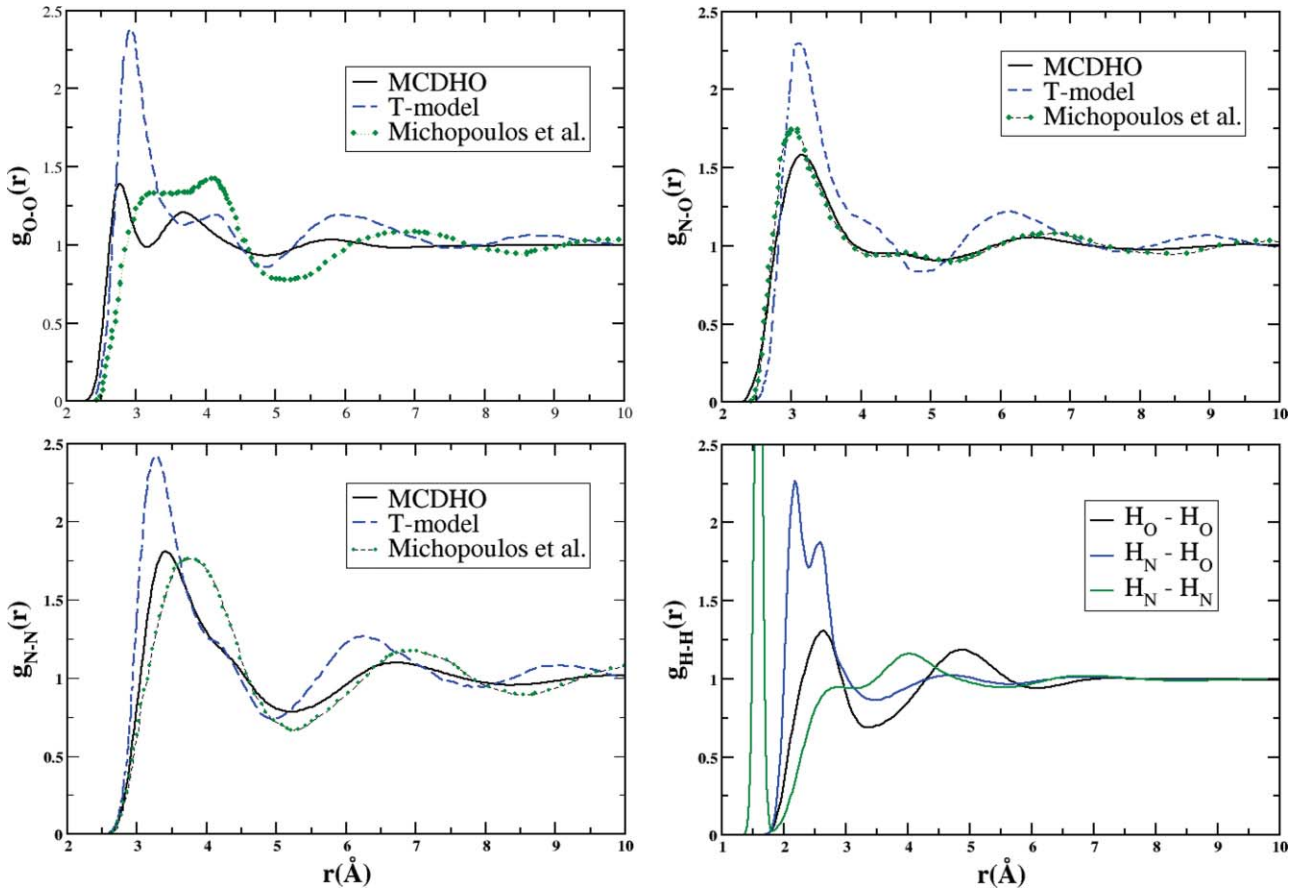

FIG. 6. Partial radial distribution functions for liquid hydroxylamine at 45 °C compared with the results of Sagarik (see Ref. 13) and Michopoulos *et al.* (see Ref. 15).

transition in condensed phase should enhance the *trans-cis* barrier. However, in the light of the results obtained in this work it is clear that, for pure hydroxylamine, the presence of the bulk in fact reduces the barrier between these conformers. Even the PCM calculation shows a substantial reduction of the barrier, a result that can be expected from the large dipole moment of the *cis* conformer. Also the analysis of the interaction of both conformers with its first neighbors shows that the *cis* conformer is forming a better H-bond network. These two factors compensate the deformation energy of the *cis* geometry and lead to the presence of both conformers in the condensed phase with almost equal probability.

We also looked into the existence of the *trans-trans* and *cis-cis* dimers in the liquid phase simulation. In a group of 500 configurations, we looked at the number of cases where the distances N–O between adjacent molecules were 2.81 ± 0.2 Å, indicating a *trans-trans* dimer, whereas a distance N–N of 3.37 ± 0.2 Å at the same time that an O–O distance of 2.86 ± 0.2 Å indicates a *cis-cis* dimer. We found that both structures occur, albeit in a small quantity (∼1.2 and 2.7 in a 500 molecules box) for such a stringent definition of distances. The relative probability of the *cis-cis* dimer is larger than that of the *trans-trans* dimer, as can be expected from the relative probability of monomers.

To investigate, if the inversion of the amino group is an alternate pathway to the transition between the *trans* and the *cis* conformers of the hydroxylamine molecule in the liquid we check if the inversion barrier is properly reproduced by the model potential. In Fig. 4, we present the deformation energy of the molecule as a function of the angle between the O–N vector and the dipole vector of the amino group. The angle of 110° corresponds to the *trans* form and 240° to the *cis* form. The 180° angle corresponds to the transition state between both the structures. As can be seen the values predicted by the model potential are slightly overestimated compared to the *ab initio* values but the transition barrier is reproduced with a good accuracy. To study the evolution of this angle in the liquid state in Fig. 5, we present the distribution of this angle during 200×10^6 configurations of a simulation of liquid hydroxylamine at 45 °C. As can be seen, the distribution of this angle is centered around a value of 112°. However, the larger value of this angle appears around 135° and does not approach the transition state for inversion that would correspond to a value of 180°. The reason for this is clear, since the value of this barrier (∼11.5 kcal/mol) is substantially larger than the rotation barrier (∼4.2 kcal/mol). Therefore, we did find that the inversion of the amino group does not constitute an alternative pathway to the transition between the *trans* and the *cis* form.

C. Structure

Figures 6 and 7 show the radial distribution functions corresponding to the liquid phase of hydroxylamine.

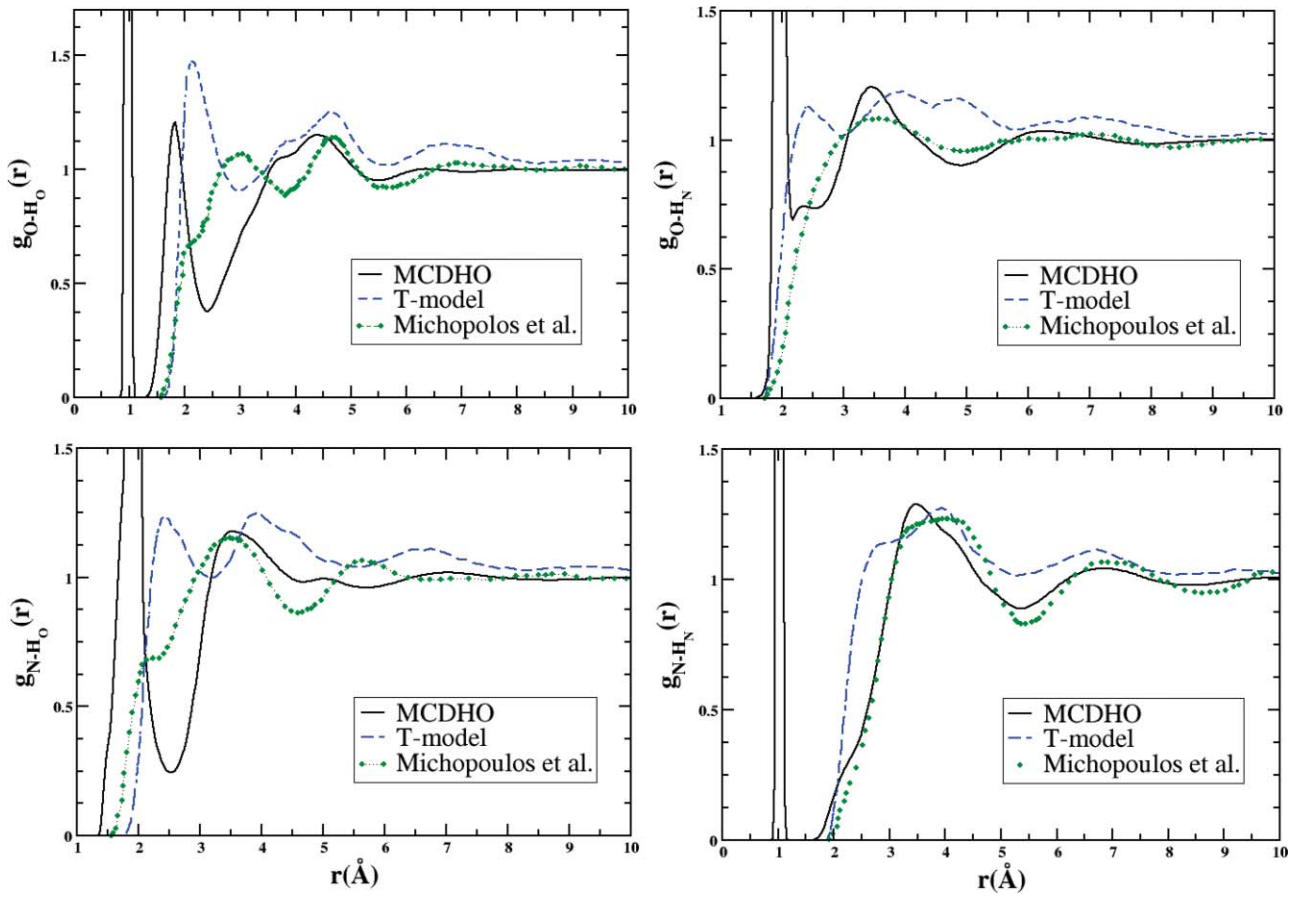

FIG. 7. Partial radial distribution functions for liquid hydroxylamine at 45 °C compared with the results of Sagarik (see Ref. 13) and Michopoulos *et al.* (see Ref. 15).

Unfortunately, there are no experimental counterparts with which to compare and thus validate the simulation, but there are previous simulations—one from Sagarik using the so called T-model[13] and other from Michopoulos *et al.*[14,15] All three simulations are presented in Figs. 6 and 7 and show considerable discrepancy. First of all and unlike the present simulation, the two previous ones do not include intramolecular relaxation and the monomer geometry that was considered corresponding to the *trans* monomer. For this reason, the very frequent structures arisen from *cis* monomer interaction in our simulation have no correspondence. Figure 6 shows the oxygen-oxygen distribution. The first noticeable fact is that the T-model predicts greater structure at short distances than the other two simulations, and this is a general trend in the radial distribution functions between heavy atoms. This indicates a more marked dimerization in this model, even though the model tends to underestimate the *ab inito* energy of the cluster interaction.[13] It is, however, consistent with the large predicted average internal energy of the liquid phase, –15.67 kcal/mol, as compared to the ∼–7 kcal/mol value in our study. As a form of validation, that work mentions that the former value is close to the sublimation energy,[39] but here we have shown that the latter value leads to the proper vaporization energy. Figure 6 compares our predicted radial distribution function between oxygens ($g_{O–O}$) and those of Sagarik[13] and Michopoulos *et al.*,[15] showing the expected differences. Our simulation predicts a peak at 2.8 Å, which corresponds to the distance involving a *cis* monomer in a dimer (see Table VI) that cannot appear in their simulation; instead, we see a broad peak around 3.5 Å. Something similar is happening in the $g_{N–O}$ function in Fig. 6, where the peak is slightly larger than that of Michopoulos *et al.*,[15] because of the presence of the *cis* monomer. Also in this figure, the curve corresponding to $g_{N–N}$ shows a narrower peak for the same reason. The heavy atom-hydrogen radial distribution functions in Fig. 7 show considerable structure for all simulations; this is due to the existence of multiple hydrogen bonding, with the curves corresponding to our simulation showing narrower peaks.

The radial distributions functions corresponding to hydrogen-hydrogen atoms are presented in Fig. 6, which again shows structure and a more marked double peak for the curve corresponding to the hydrogens from the nitrogen vs. the hydrogens of the hydroxyl. Looking into the distances between hydrogen atoms presented in Table VI allows for an interpretation of these radial distribution functions. The $g_{HN–HO}$ presents a marked peak at ∼2.2 Å and, from Table VI, we can see that this distance is closer to that of the *cis-cis* dimer. The $g_{HO–HO}$ shows a peak at ∼2.5 Å, which corresponds to the *cis-cis* dimer, and no structure is found at ∼2.0 Å, the distance of the *trans-trans* or *trans-cis* dimers. Finally, the $g_{HN–HN}$ shows structure only at ∼4.0 Å, a distance that could correspond to dimers made with *trans* monomers, but no structure corresponding to ∼2.5 Å of the *cis-cis* dimer. This seems to contradict the previous findings

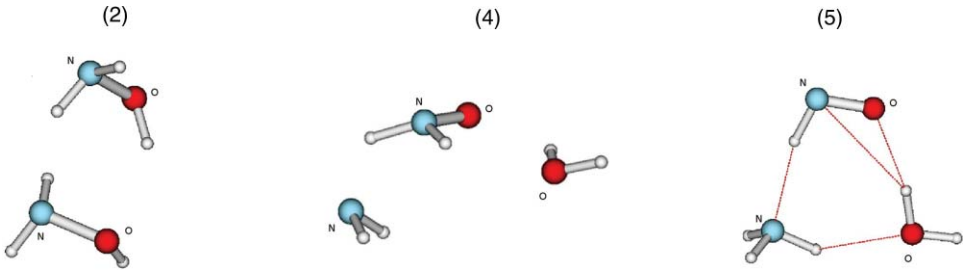

FIG. 8. Decomposition pathway from the hydroxylamine *cis-cis* dimer (2) through the transition state (4) leading to the products (5) proposed by Nast *et al.*[1]

but can be explained if we consider that in the *cis-cis* structure 2 of Fig. 2 there would be a rotation around the N–O axis, allowing the nitrogen's hydrogens to bond with the surrounding molecules, producing an increase in the H_N–H_N distances.

D. Decomposition

The decomposition of hydroxylamine is an important matter, since it makes the substance difficult to handle and has even lead to tragic industrial accidents.[5,42] Even the thermal decomposition hazard of hydroxylamine/water mixtures has been established.[6] A long time ago, Nast and Foppl[1] proposed the following reaction scheme for decomposition based on the experimental determination of the products:

$$2NH_2OH \rightarrow H_2O + NH + HNO.$$

However, this scheme was discarded in a recent study of the thermal decomposition pathways of hydroxylamine.[12] The transition state of this bimolecular path could not be found, suggesting that the pathway involved multiple steps, and an alternative pathway was proposed. It was found that hydration of the alternative pathway decreased the energy of both the transition state barrier and the products, but no exothermicity was found. The reactant considered, however, was a dimer of *trans* monomers based on the greater stability of these monomers in the gas phase. The whole picture could be different if we started with a *cis-cis* dimer as found in the liquid phase. In order to test this idea we considered the decomposition pathway free energies, starting from the minimum energy *cis-cis* dimer. This was done in the following manner. Starting from the minimum-energy *cis-cis* dimer configuration, we elongated the oxygen-hydrogen and nitrogen-hydrogen distances in the hydrogen-bond positions of the dimer. The nitrogen-oxygen distance was also elongated in the acceptor monomer. An energy minimization was performed from this configuration that converges to the products' minimum-energy configuration. Once we had obtained the reactants (*cis-cis* dimer) and the products minimum-energy configuration we performed a QST2 optimization with GAUSSIAN09. An additional QST3 optimization was needed, since the QST2 does not converge to the desired transition state. The initial guess of the transition state for the QST3 optimization was the final configuration yielded by the QST2 optimization.

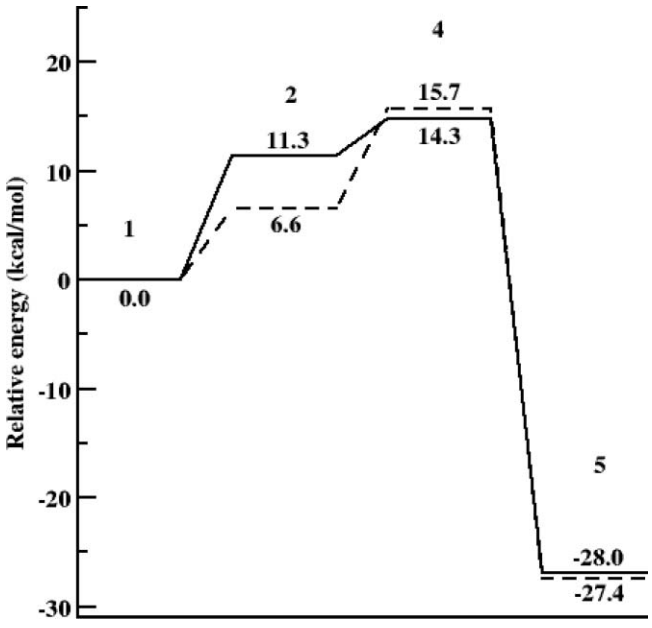

FIG. 9. Decomposition pathway free energies from the hydroxylamine *cis-cis* dimer (2), through the transition state (4) leading to the products (5) proposed by Nast *et al.* (Ref. 1). The *trans-trans* monomer (1) is given as a reference. The numeration corresponds to Figs. 2 and 6. Full lines correspond to vacuum calculation and the broken lines to those performed with the PCM solution model (Ref. 41). The free energies reported are those calculated by the GAUSSIAN09 (Ref. 24) program in the thermochemistry analysis of a frequency calculation. The analysis uses the standard expressions for an ideal gas in the canonical ensemble and it includes the enthalpy and entropic contributions.

The resulting decomposition is presented in Fig. 8, where the products are exactly those of the Nast and Foppl scheme. It must be mentioned that, from the transition state, one easily goes to the products but not to the reactants. Still, we must remember that the *cis-cis* dimer is 11.5 kcal/mol above the *trans-trans* dimer in the gas phase. A scheme of the relative free energies of the pathway is shown in Fig. 9. It is clear that there is a small barrier from step 2 to step 3 and large exothermicity to step 4. We repeated the scheme with the PCM model for inclusion of the solvent effect[41] and found that the difference between step 1 and step 2 is diminished but it remains large, indicating that molecularity of the interaction is important in order to favor step 2. On the other hand, the energy of the transition state and the exothermicity are not affected by the PCM. Given these results we can conclude that the abundant existence of *cis* monomers in the liquid phase is behind the easy and exothermic decomposition of hydroxylamine at room temperature.

IV. CONCLUSIONS

We have presented a detailed study including *ab initio* calculations and classic Monte-Carlo simulations of

hydroxylamine in the gas and liquid phases. Substantial care went into constructing the classical interaction potentials in order to ensure that the *ab initio* results at the MP2 level were reproduced adequately. In fact, we had to include an additional charge density in the oxygen atom. An analytical model potential which includes polarizability, many-body effects, and intramolecular relaxation was constructed to ensure both an accurate reproduction and a reliable description of the liquid phase. Since different conformers of the monomer appear in the gas and liquid phases, it was critical to allow for the proper molecular description of the compound. The results of the simulation were compared to available experimental data in order to validate the model; the comparison yielded good agreement, so there is confidence regarding the results and the molecular analysis performed. Our study leads us to conclude that the liquid hydroxylamine has a multitude of hydrogen bonds leading to a large density where the existence of *cis* conformers and clusters of these conformers is possible. This allows for the occurrence of the classical Nast and Foppl[1] scheme for the molecule's decomposition at room temperature and explains its large exothermicity and instability.

ACKNOWLEDGMENTS

We want to thank Reyes García Carreón for his support in the computational aspect of this work and acknowledge the financial support of DGAPA under Grant No. IN122809 and CONACyT under Grant No. 128575. Computer resources from the Centro Nacional de Supercómputo from the Instituto Potosino de Investigación Científica y Tecnológica (IPICyT), San Luis Potosí, México, are also acknowledged.

[1]R. Nast and I. Z. Foppl, Z. Anorg. Allg. Chem. **263**, 310 (1950).
[2]W. P. Jencks, *Catalysis In Chemistry And Enzymology* (McGraw-Hill, New York, 1969).
[3]K. Jones, *Comprehensive Inorganic Chemistry* (Pergamon, New York, 1973) Vol. 2.
[4]Manuf. Chemist Aerosol News **35**, 29 (1964).
[5]L. A. Long, Process Safety Progress **23**, 114 (2004).
[6]C. Wei, S. R. Saraf, W. J. Rogers, and M. S. Mannan, Thermochim. Acta **421**, 1 (2004).
[7]G. A. Yeo and T. A. Ford, J. Mol. Struct. **141**, 331 (1986).
[8]G. A. Yeo and T. A. Ford, J. Mol. Struct. **217**, 307 (1990).
[9]G. A. Yeo and T. A. Ford, Chem. Phys. Lett. **178**, 266 (1991).
[10]G. A. Yeo and T. A. Ford, J. Mol. Struct. **270**, 417 (1992).
[11]G. A. Yeo and T. A. Ford, Spectrochim. Acta **50A**, 5 (1994).
[12]Q. Wang, C. Wei, L. M. Perez, W. J. Rogers, and M. B. Hall, J. Phys. Chem. A **114**, 9262 (2010).
[13]K. Sagarik, J. Mol. Struct.: Theochem **465**, 141(1999).
[14]Y. Michopoulos, P. Botschwina, and B. M. Rode, Z. Naturforsch., A: Phys. Sci. **46**, 32 (1991).
[15]Y. Michopoulos and M. Rode, Phys. Scr. **38**, 84 (1991).
[16]H. Saint-Martin, J. Hernández-Cobos, M. Bernal-Uruchurtu, I. Ortega-Blake, and H. J. C. Berendsen, J. Chem. Phys. **113**, 10899 (2000).
[17]J. Hernández-Cobos, H. Saint-Martin, A. D. Mackie, L. F. Vega, and I. Ortega-Blake, J. Chem. Phys. **123**, 044506 (2005).
[18]M. Carrillo-Tripp, H. Saint-Martin, and I. Ortega-Blake, J. Chem. Phys. **118**, 7062 (2003).
[19]M. L. San-Román, M. Carrillo-Tripp, H. Saint-Martin, J. Hernández-Cobos, and I. Ortega-Blake, Theor. Chem. Acc. **115**, 177 (2006).
[20]R. Ayala, J. M. Martínez, R. R. Pappalardo, H. Saint-Martin, I. Ortega-Blake, and E. Sánchez-Marcos, J. Chem. Phys. **117**, 19512 (2002).
[21]R. Ayala, J. M. Martínez, R. R. Pappalardo, and E. Sánchez-Marcos, J. Chem. Phys. **121**, 7269 (2004).
[22]M. Valdéz-González, H. Saint-Martin, J. Hernández-Cobos, R. Ayala, E. Sánchez-Marcos, and I. Ortega-Blake, J. Chem. Phys. **127**, 224507 (2007).
[23]J. Hernández-Cobos, M. C. Vargas, A. Rámirez-Solís, and I. Ortega-Blake, J. Chem. Phys. **133**, 114501 (2010).
[24]M. J. Frisch, G. W. Trucks, H. B. Schlegel, *et al.*, GAUSSIAN 09, Revision A.01, Gaussian, Inc., Wallingford, CT, 2009.
[25]J. Kim and K. S. Kim, J. Chem. Phys. **109**, 5886 (1998); K. S. Kim, P. Tarakeshwar, and J. Y. Lee, Chem. Rev. **100**, 4145 (2000); A. Shank, Y. Wang, A. Kaledin, B. J. Braams, and J. M. Bowman, J. Chem. Phys. **130**, 144314 (2009).
[26]D. Hankins, J. Moskowitz, and F. Stillinger, J. Chem. Phys. **53**, 4544 (1970).
[27]N. Pastor and I. Ortega-Blake, J. Chem. Phys. **99**, 7899 (1993).
[28]M. I. Bernal-Uruchurtu and I. Ortega-Blake, J. Chem. Phys. **103**, 1588 (1995).
[29]M. I. Bernal-Uruchurtu, J. Hernández-Cobos, and I. Ortega-Blake, J. Chem. Phys. **108**, 1750 (1998).
[30]V. F. Lotrich and K. Szalewicz, J. Chem. Phys. **106**, 9668 (1997).
[31]S. Tsunekawa, J. Phys. Soc. Jpn. **33**, 167 (1972).
[32]D. Luckhaus, J. Chem. Phys. **120**, 8409 (1997).
[33]R. Withnall and L. Andrews, J. Phys. Chem. **92**, 2155 (1988).
[34]N. Metropolis, A. W. Rosenbluth, M. N. Rosenbluth, A. H. Teller, and E. Teller, J. Chem. Phys. **21**, 1087 (1953).
[35]K. Hastings, Biometrika **57**, 97 (1970).
[36]L. Martínez, R. Andrade, E. G. Birgin, and J. M. Martínez, J. Comput. Chem. **30**(13), 2157 (2009).
[37]H. Flyvbjerg and H. G. Petersen, J. Chem. Phys. **91**, 461 (1989).
[38]M. P. Allen and D. J. Tildesley, *Computer Simulations Of Liquids* (Oxford Science, Oxford, 1987).
[39]R. A. Back and J. Betts, Can. J. Chem. **43**, 2157 (1965).
[40]S. Miertuš, E. Scrocco, and J. Tomasi, Chem. Phys. **55**, 117 (1981).
[41]S. Visozo and B. M. Rode, Chem. Phys. **199**, 129 (1995).
[42]M. Reisch, Chem. Eng. News **77**(99), 11 (1999).
[43]See supplementary material at http://dx.doi.org/10.1063/1.3610344 for all the *ab initio* energies and a description of the model potential.